

JGR Space Physics

RESEARCH ARTICLE

10.1029/2020JA028635

Key Points:

- Plasmaspheric hiss waves are more spatially and temporally coherent at low- L , and are incoherent where $L > \sim 4.5$
- Plasmaspheric hiss becomes incoherent when spacecraft separation is greater than 0.23 RE or ~ 10 min inside of $L \sim 4.5$
- Our results show that the timescale and spatial scales of plasmaspheric hiss are significantly less than previously thought

Supporting Information:

- Supporting Information S1

Correspondence to:

A. W. Degeling,
degeling@sdu.edu.cn

Citation:

Zhang, S., Rae, I. J., Watt, C. E. J., Degeling, A. W., Tian, A., Shi, Q., et al. (2021). Determining the temporal and spatial coherence of plasmaspheric hiss waves in the magnetosphere. *Journal of Geophysical Research: Space Physics*, 126, e2020JA028635. <https://doi.org/10.1029/2020JA028635>

Received 28 AUG 2020

Accepted 11 JAN 2021

Determining the Temporal and Spatial Coherence of Plasmaspheric Hiss Waves in the Magnetosphere

Shuai Zhang^{1,2} , I. Jonathan Rae^{1,2,3} , Clare E. J. Watt^{3,4} , Alexander W. Degeling¹ , Anmin Tian¹ , Quanqi Shi¹ , Xiao-Chen Shen⁵ , Andy W. Smith² , and Mengmeng Wang¹ 

¹Shandong Provincial Key Laboratory of Optical Astronomy and Solar-Terrestrial Environment, Institute of Space Sciences, Shandong University, Weihai, China, ²Mullard Space Science Laboratory, University College London, Dorking, London, UK, ³Department of Maths, Physics and Electrical Engineering, Northumbria University, Newcastle, UK, ⁴Department of Meteorology, University of Reading, Reading, UK, ⁵Center for Space Physics, Boston University, Boston, MA, USA

Abstract Plasmaspheric hiss is one of the most important plasma waves in the Earth's magnetosphere to contribute to radiation belt dynamics by pitch-angle scattering energetic electrons via wave-particle interactions. There is growing evidence that the temporal and spatial variability of wave-particle interactions are important factors in the construction of diffusion-based models of the radiation belts. Hiss amplitudes are thought to be coherent across large distances and on long timescales inside the plasmapause, which means that hiss can act on radiation belt electrons throughout their drift trajectories for many hours. In this study, we investigate both the spatial and temporal coherence of plasmaspheric hiss between the two Van Allen Probes from November 2012 to July 2019. We find $\sim 3,264$ events where we can determine the correlation of wave amplitudes as a function of both spatial distance and time lag in order to study the spatial and temporal coherence of plasmaspheric hiss. The statistical results show that both the spatial and temporal correlation of plasmaspheric hiss decrease with increasing L -shell, and become incoherent at $L > \sim 4.5$. Inside of $L = \sim 4.5$, we find that hiss is coherent to within a spatial extent of up to $\sim 1,500$ km and a time lag up to ~ 10 min. We find that the spatial and temporal coherence of plasmaspheric hiss does not depend strongly on the geomagnetic index (AL^*) or magnetic local time. We discuss the ramifications of our results with relevance to understanding the global characteristics of plasmaspheric hiss waves and their role in radiation belt dynamics.

1. Introduction

Whistler mode hiss is a broadband (~ 50 – $2,000$ Hz) unstructured electromagnetic emission typically occurring inside the plasmasphere and the plasmaspheric plumes (Chan & Holzer, 1976; Hayakawa et al., 1986; Parrot & Lefeuvre, 1986). Hiss plays an important role in radiation belt dynamics via gyro-resonant wave-particle interactions (Dunckel & Helliwell, 1969; Meredith et al., 2004; R. M. Thorne et al., 1973). These wave-particle interactions break all three adiabatic invariants, leading to the pitch angle diffusion and potential loss of electrons to the upper atmosphere (J. Li et al., 2019; Ni et al., 2013, 2014; Summers et al., 2007a, 2007b; R. M. Thorne et al., 2013). Plasmaspheric hiss is largely responsible for the formation of the slot region between the inner and outer radiation belts through the cyclotron resonant pitch angle diffusion (e.g., Lyons & Thorne, 1973; Meredith et al., 2009).

Traditionally, empirical models of pitch angle diffusion in the radiation belts have been computed using average magnetospheric parameters, such as number density and magnetic field intensity (e.g., Fok et al., 2011; Glauert et al., 2013; Malaspina et al., 2020; Subbotin & Shprits, 2009). However, recent modeling and data analysis work (Watt et al., 2019, 2021) indicates that the efficacy of diffusion is increased if the variability in hiss wave growth parameters is considered instead of simply using average values. In idealized numerical experiments of radial diffusion, the solution is shown to depend upon the temporal and length scales of variability in the diffusion coefficients (Thompson et al., 2020). Therefore, in general, it is important to know how rapidly wave and plasma characteristics vary in order to determine the importance of variability, and the best way to construct models of diffusion coefficients, for all types of wave-particle interactions in the Outer Radiation Belt.

The wave coherence spatial scale in radiation belt region has been studied in depth (e.g., Agapitov et al., 2010; Blum et al., 2016; Gurnett et al., 1979; Němec et al., 2016; Santolík & Gurnett, 2003). For example, Shen et al. (2019) statistically obtained the spatial correlation scale of chorus wave of 315 km between L shells of ~ 5 –6. Using a case study, J. Li et al. (2017) found that there is a good correlation between the whistler mode waves outside the plasmasphere and the hiss waves inside the plasmasphere, and that for 500–1,500 Hz rising-tone emissions, their coherence was unexpectedly large at spatial scales up to $4.3 R_E$ and even across the plasmapause. For the focus of this study, plasmaspheric hiss, Agapitov et al. (2018) statistically analyzed the radial separation (Δr) effect on the correlation of hiss wave amplitudes using five THEMIS spacecraft observations. Agapitov et al. (2018) found that the radial correlation of hiss waves decays to 0.5 at radial separation $\Delta r \sim 3,000$ km. However, many outstanding questions regarding the global temporal and spatial coherence of hiss wave still remain, for example: (a) what is the spatial coherence of plasmaspheric hiss wave in a physical coordinate system? (b) does the spatial coherence vary with L shell or magnetic local time (MLT)? (c) what is the temporal coherence of plasmaspheric hiss waves?

In this study, we study the spatial and temporal variation of hiss using Van Allen Probes measurements. The Van Allen probes provide measurements of hiss waves at constantly varying separation from ~ 0.01 to $5 R_E$, since Van Allen Probe A catches up and passes Van Allen Probe B every few weeks, making the mission a perfect platform for this type of analysis. We study the correlation of wave amplitudes across a range of frequencies that cover the plasmaspheric hiss band as a function of spacecraft separation and time lag in order to determine how rapidly the correlations vary as the satellite separation and time lag increases.

The remainder of this study is organized as follows. In Section 2, we discuss the data set, selection criteria and the correlation analysis method of the plasmaspheric hiss. Section 3 shows the statistical results of the spatial and temporal correlations of the plasmaspheric hiss. The discussion and conclusion are shown in Sections 4 and 5.

2. Data Set and Methods

The Van Allen Probes were launched on August 30, 2012 and consists of two identical satellites (Van Allen Probes A & B) in elliptic orbits (a perigee of 618 km, an apogee of $5.8 R_E$, and 10.2° orbital inclination) with ~ 537 min orbital period (Mauk et al., 2012). The measurements used in this study are primarily obtained from Electric and magnetic field instrument suite and integrated science (EMFISIS; Kletzing et al., 2013), which consists of ~ 6 s resolution wave magnetic field data in 65 frequency channels (~ 10 – $12,000$ Hz) from WaveForm Receiver (WFR). The WFR also provides the wave normal angle, polarization and ellipticity calculated by the singular value decomposition method (Santolík et al., 2003). The electron density data used in this study are derived from the upper hybrid frequency from the high-frequency receiver spectra (Kurth et al., 2015).

Figure 1 shows an example of a hiss event from Van Allen Probe A on November 9, 2012 and how we select our hiss intervals. Briefly, we select hiss waves that are inside the plasmasphere using previously published criteria, as outlined below, when:

- i. Both the electron density measurements from Van Allen Probes A&B are higher than the larger value between $10 \times (6.6/L)^4$ and 50 cm^{-3} (the black line in Figure 1a) to ensure that the observations are in the plasmasphere (e.g., Li et al., 2010, 2015). For the vast majority of this event, the observed value is larger than the black line and hence most observations during this event fit this criterion.
- ii. The wave is broadband in the frequency range of 50–2,000 Hz (Figure 1b). This is detected by ensuring that the majority of large-amplitude regions (with a power spectral density greater than $10^{-7.5} \text{ nT}^2/\text{Hz}$) stay in this hiss frequency band. Large amplitude events are studied in order to ensure the correlation analysis is focused on the plasmaspheric hiss activity, and not background noise or other signals that are more ambiguous in origin. For this event, there are several emissions around 13:00–15:00 UT and 16:00–19:00 UT that do not fit this criterion, but all over wave amplitudes during this event fall in between the horizontal black lines.
- iii. The planarity is larger than 0.2 (Figure 1c) and ellipticity larger than 0.7 (Figure 1d) over the frequency range of 50–2,000 Hz. The magnetosonic waves, which typically have very low ellipticity approaching zero, will likely be excluded in this step (e.g., Kim et al., 2019; Ma et al., 2016). For this event, all wave

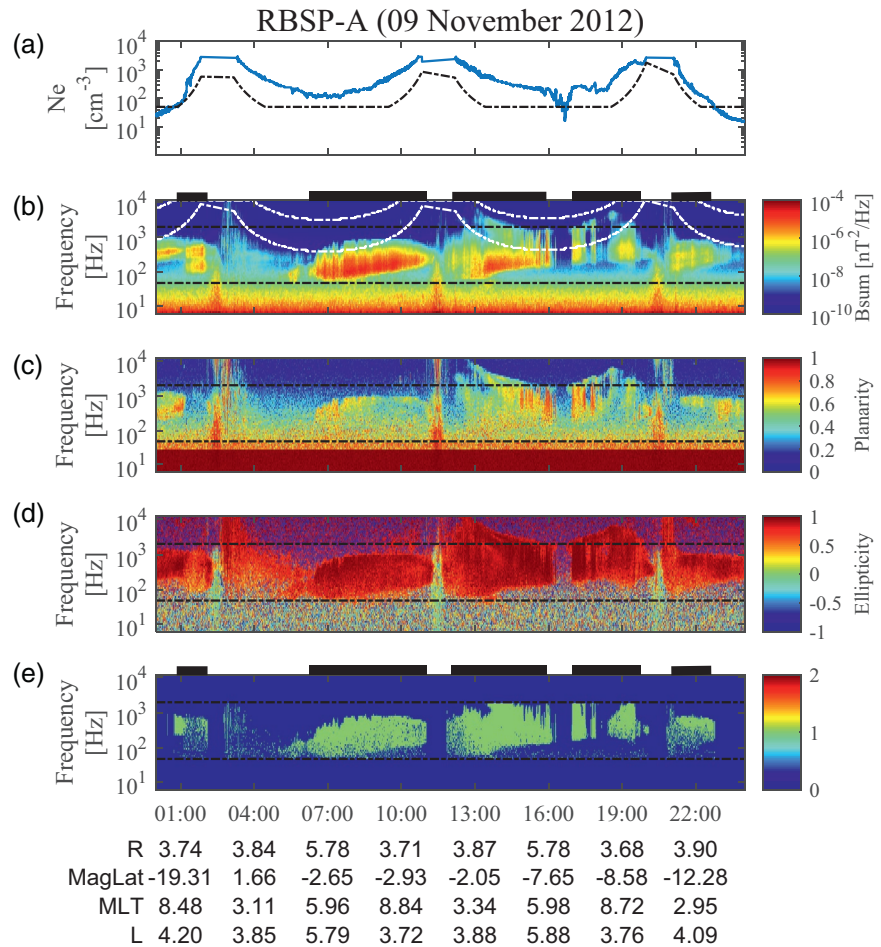


Figure 1. An example of the density and wave survey data measured by Van Allen Probes A on November 09, 2012 from 00–24 UT. (a) Electron density derived from the upper hybrid frequency data (blue line), the black line indicates the larger value between $10 \times (6.6/L)^4$ and 50 cm^{-3} ; (b) magnetic field wave power spectrogram; (c) planarity; (d) ellipticity; (e) bins that meet the criteria from (i) to (iv) are green. The two black lines in panels (b–e) indicate frequencies of 50 Hz and 2 kHz. The two white dashed lines in (b) indicate frequencies of $0.1 f_{ce}$ and $0.8 f_{ce}$, where f_{ce} is the electron cyclotron frequency. The black bars above the panels (b and e) indicate the duration of plasmaspheric hiss.

- amplitudes in the studied frequency range adhere to these criteria other than waves during perigee, as denoted by vertical striped emissions that extend across all of the frequency range.
- iv. Chorus waves are also excluded, which are typically observed in the plasmatrough region (where the black line is higher than the blue line in Figure 1a), and the majority of large-amplitude regions stay in 0.1 and $0.8 f_{ce}$ (the two white lines in Figure 1b), where f_{ce} is the equatorial electron gyrofrequency (e.g., Burtis & Helliwell, 1969; Tsurutani & Smith, 1974). Finally, we perform a visual inspection of each event to ensure that even chorus waves that penetrate the plasmasphere (e.g., Chen et al., 2012; Zeren et al., 2013) are excluded from our data set.
 - v. Finally, the satisfied bins are shown in green in Figure 1e. The example of the duration of plasmaspheric hiss is shown as the black bars at the top of Figures 1b and 1e, showing that the vast majority of large-amplitude, broadband plasmaspheric hiss is captured by these criteria.

An example of the correlation analysis of the plasmaspheric hiss waves is shown in Figure 2. Figures 2a and 2b show the magnetic field spectrograms of wave power from Van Allen Probes A&B, which are in a similar format as that of Figure 1b. Figure 2c shows the integrated hiss wave amplitudes of Van Allen Probes A (red) & B (blue), which are calculated by integrating the power spectral densities in panels a and b across the frequency range between 50 Hz and 2 kHz and taking the square root value. Figure 2d shows the spatial separation (Δd) between Van Allen Probes A&B. Figure 2e shows the time lag between Van Allen Probes

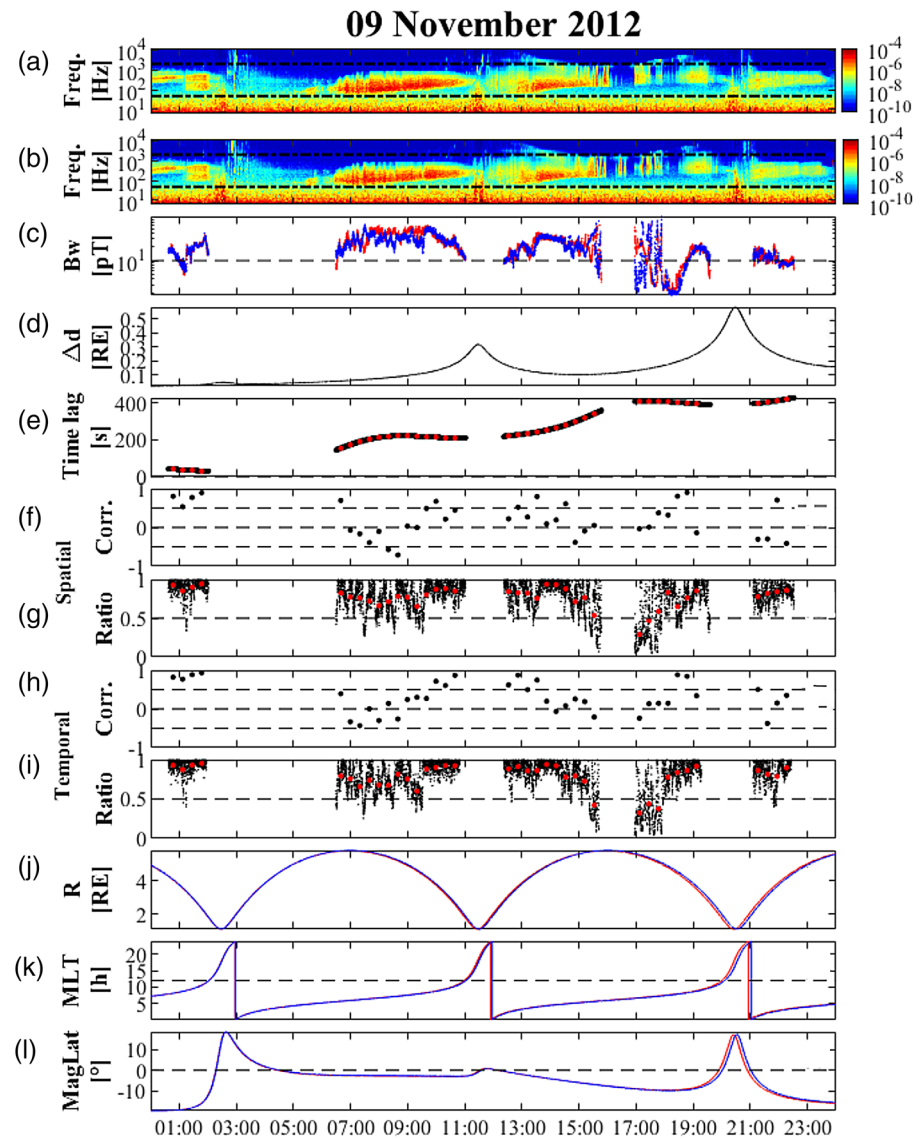


Figure 2. An example of the correlation of the plasmaspheric hiss waves observed from Van Allen Probes A & B. (a and b) Magnetic field wave power spectrogram measured from Van Allen Probes A & B; (c) Wave magnetic amplitudes integrated from 50–2,000 Hz of Van Allen Probes A (red) and B (blue); (d) spacecraft separation; (e) spacecraft time lag; (f and g) spatial correlation coefficients and ratios of amplitudes (smaller amplitudes/larger amplitudes); (h and i) temporal correlation coefficients and ratios of amplitudes; (j) radial distance from earth; (k) magnetic local time (MLT); (l) magnetic latitude (MLAT). The red dots in panels (e, g, and i) are 20 min averaged values of the black dots.

A&B, which are estimated from the spacecraft location in Figures 2j–2l. Figures 2f and 2g show the spatial correlation coefficients and ratios between the red and blue lines in panel c (two time series of amplitudes at same time but different position) in steps of 20 min. Figures 2h and 2i show the temporal correlation coefficients and ratios between the shifted blue line (with the time lag in Figure 2e) and red line (Figure 2c) (two time series of amplitudes at same position but different time with the time lag). In total, 3,264 events were found during November 2012 to July 2019, where both Van Allen Probes A&B observed hiss wave with small separation ($<1 R_E$). Each event is determined as a 20 min time window.

It can be seen in Figures 2a and 2b that the hiss spectra appear to be relatively well correlated visually. Figure 2c demonstrates that the integrated wave amplitudes during the identified hiss wave intervals (all other wave amplitudes are excluded) also appear well matched both in shape and in amplitude. Figures 2d and 2e show the differing spacecraft separation and corresponding time lag that goes into our analysis. Figures

2f and 2g show the correlation coefficient and amplitude ratio, respectively, between the two time series in Figure 2c but accounting for the spacecraft separation shown in Figure 2d, which shows that there is a clear variability to the correlation as a function of time throughout the interval. Similarly Figures 2h and 2i show the same cross-correlation and amplitude, respectively according to the time lag between spacecraft shown in Figure 2e. Again there is clear variability in the correlation and amplitude ratio seen in Figure 2h. Taken together, the spatial and temporal correlations in Figures 2f and 2h (respectively) show that there are periods where there is excellent spatial and temporal agreement between the spacecraft (e.g., 13:00 UT), but that there are also very poor correlations (e.g., 17:00 UT).

3. Statistical Results

3.1. Event Distribution

Figure 3 shows the relevant characteristics of hiss events as a function of location and separation. The left hand column shows a scatterplot of each of the 3,264 events, whereas the right hand column shows a two-dimensional histogram of these events. Figure 3a shows the relevant locations of plasmaspheric hiss events in MLT- L coordinates and Figure 3b shows their corresponding two-dimensional histograms, where the color represents the number of events in each bin. We can see that our events have a peak in occurrence in the post-noon sector around $L = 6$, but have a good distribution (>10 points) in the dayside magnetosphere between $2 < L < 6$. Figures 3c and 3d show the event distributions of the *total* spacecraft separation (Δd) between Van Allen probes A&B as a function of L -shell. We can see that at large L -shells ($L = 6$) there is a uniform coverage at all spacecraft separations, but that at lower L -shells the occurrence peaks in the 4,000–600 km range, although there is still good coverage at $L < 4$. Figures 3e and 3f show the event distributions of the azimuthal separation (ΔMLT) between Van Allen probes A&B as a function of L -shell. We can see that there is generally little separation in MLT between the two spacecraft but if there is, this is limited to ± 1 MLT. Figures 3g and 3h show the event distributions of the *radial* separation (ΔL) between Van Allen probes A&B as a function of L -shell. We can see that the measurements are mostly distributed in $|\Delta MLT| < 1$ h and $|\Delta L| < 0.5$, and all of the spacecraft separations (Δd , ΔMLT , and ΔL) are decreasing with increasing L -shell. Finally, Figures 3i and 3j show the distributions of hiss waves in ΔMLT - ΔL panel. We can see that there is a large concentration of occurrences close to $\Delta MLT = 0$ and $\Delta L = 0$, but that there is a large spread and where the spacecraft separation is larger, the MLT is larger. However, the highest number of events is highest near $\Delta MLT < 0.2$ h and $\Delta L < 0.2$.

3.2. Spatial Correlation of Plasmaspheric Hiss

Figures 4a–4d shows spatial correlation coefficients in Figure 2f as a function of L -shell for all of 3,264 events during November 2012 to July 2019. Figure 4a shows a scatterplot of the spatial correlation coefficients shown in Figures 2f and 4b shows a two-dimensional histogram. Figure 4c shows the normalized probability for each column, where the largest bin in each column is normalized to 1. Finally, the bilinear interpolated probability distributions are shown in Figure 4d, and the red solid line indicates the least squares fitting to the contours (red line). It can be seen that the spatial correlation coefficients of amplitudes are higher at smaller L -shell than larger L -shell, which means that the plasmaspheric hiss is more spatially incoherent with increasing L -shell. A correlation of 0.5 is reached at $L = 3.34$, demonstrating that only 25% of the variance of the data set is explained by the L -shell relationship and that correlations between Van Allen Probe measurements of hiss become very weak at this location.

Figures 4e–4h shows spatial correlation coefficients as a function of the separation of Van Allen Probes A&B, Δd , for all of 3,264 events, which have same format with panels a–d and on a log-linear scale. From panels e and f, we can see that only few ($\sim 8\%$) spatial correlation coefficients at $\Delta d < 1$ are greater than 0.8, and there are fewer events distributed in the lower left part of the Figure. From Figures 4g and 4h, it can be seen that as separation increase, the spatial correlation coefficients of amplitudes decreased significantly, which means that the plasmaspheric hiss is more incoherent with increasing separation. To quantify the variation of spatial correlation with increased Δd , we fit a functional form to the contours (black line) in Figure 4h. Considering that the correlation coefficients vary from ~ 1 at $\Delta d \sim 0$ to 0 as Δd gets

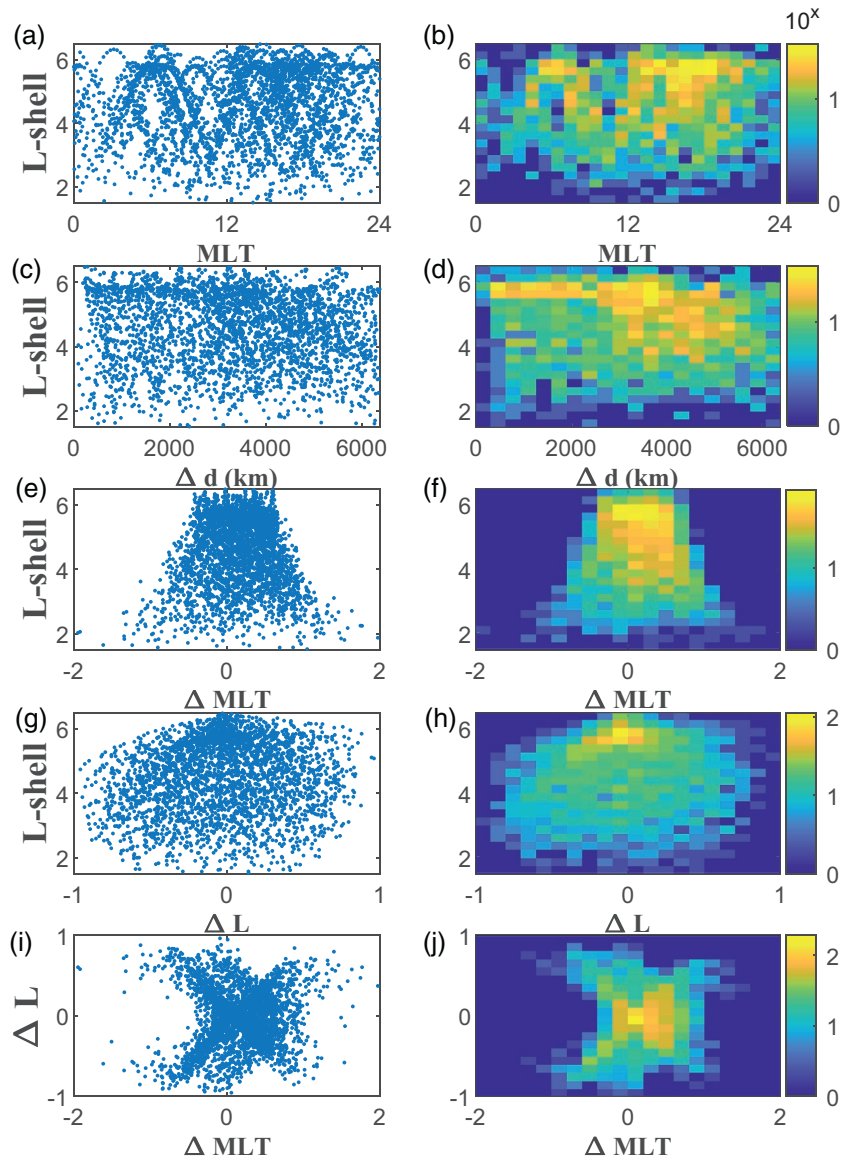


Figure 3. The distribution of plasmaspheric hiss in the (a) MLT- L , (c) Δd - L , (e) Δ MLT- L , (g) ΔL - L , and (i) Δ MLT- ΔL planes. MLT and L are the measurements from the Van Allen Probes A. Δd , Δ MLT and ΔL indicate the total, azimuthal, and radial separation between Van Allen probes A& B. Right panels show the corresponding two-dimensional histograms of the events in left panels. MLT, magnetic local time.

very large, we choose $f(\Delta d) = e^{k\Delta d}$ to fit the peaks in spatial correlation, indicated by the red dotted line, where $k = -6.68 \times 10^{-04}$ ($R^2 = 0.67$). We find that the spatial correlation coefficients drop to 0.5 when $\Delta d \sim 1,038$ km. If we consider when the correlation coefficients drop to 0.3 or 0.1, we obtained values of Δd of 1,803 and 3,448 km, respectively. In summary, we find that the spatial coherence of plasmaspheric hiss is much smaller than previously thought, and statistically meaningful correlations may only last $\sim 1,000$ km. Figure S1a-S1d demonstrates that the ratio of plasmaspheric hiss amplitude (see Figure 2g) decreases significantly as spacecraft separation increases.

To examine the combined L -shell and Δd effect, Figure 5a shows the distributions of the spatial correlation coefficients as a function of the spacecraft separation Δd and L -shell. The color indicates the median value of the spatial correlation coefficients in each bin. Figure 5b shows the interpolated distributions in panel a, and the red (black) lines indicate the 0.5 (0.1) contours. We can see that when $L < \sim 4.5$, the spatial

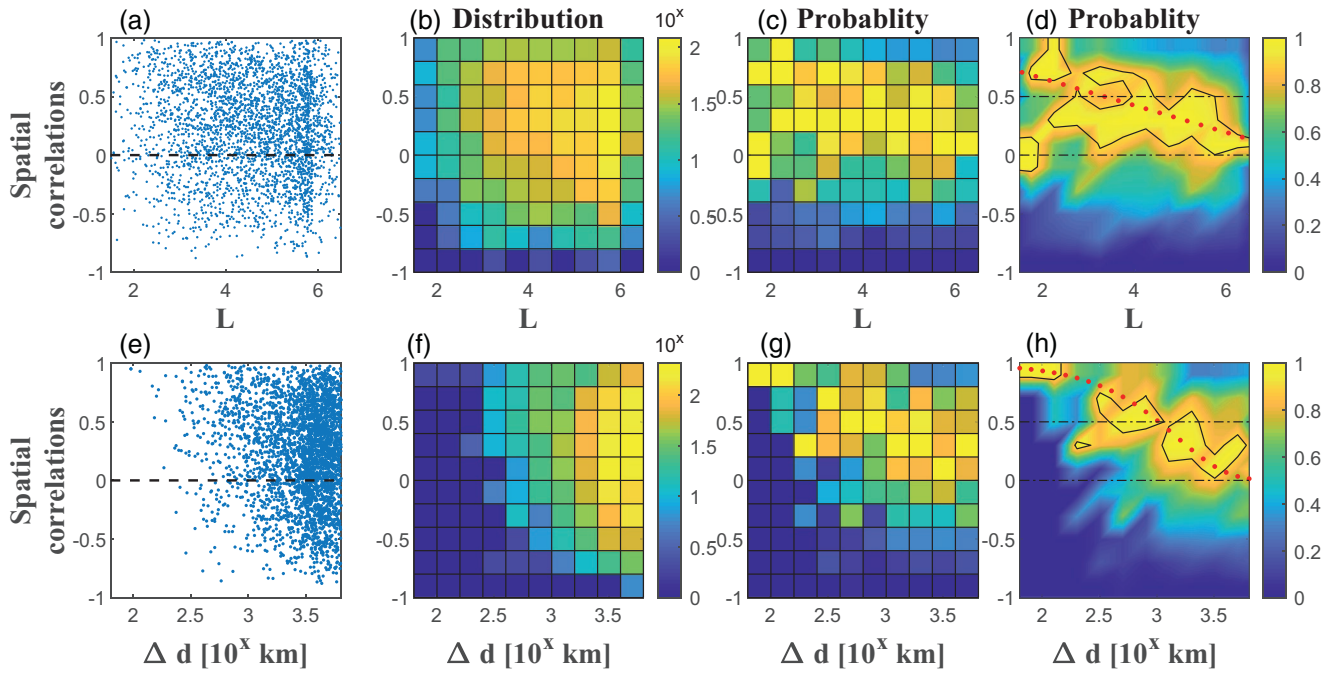


Figure 4. The distributions of the spatial correlation coefficients. (a) The scatterplot of the spatial correlation coefficients against L -shell. (b) The number distribution of the events in panel a. (c) The column normalized probability distribution in each given L -shell bin, the largest bin in each column is normalized to 1. (d) The interpolated figure to panel (c), the black solid line indicates 0.9 contours. Panels (e–h) show the distributions of the spatial correlation coefficients against the spacecraft separation between Van Allen Probes A & B, which have the same format as in panels (a–d). The red lines indicate the least squares fitting and the weighted fitting ($f(x) = e^{k\Delta d}$) to the contours in panels d and h, respectively.

correlation coefficient is very high when Δd is small, and it decreases significantly as Δd increases along the y-axis (and drop to 0.5 at average $\Delta d \sim 1,500$ km). When $L > \sim 4.5$, no matter what Δd and L -shell, all of the coefficients at any separation are significantly reduced and closer to 0 than 1, with an average of ~ 0.3 .

In summary, we find that plasmaspheric hiss is incoherent ($R^2 < 0.5$):

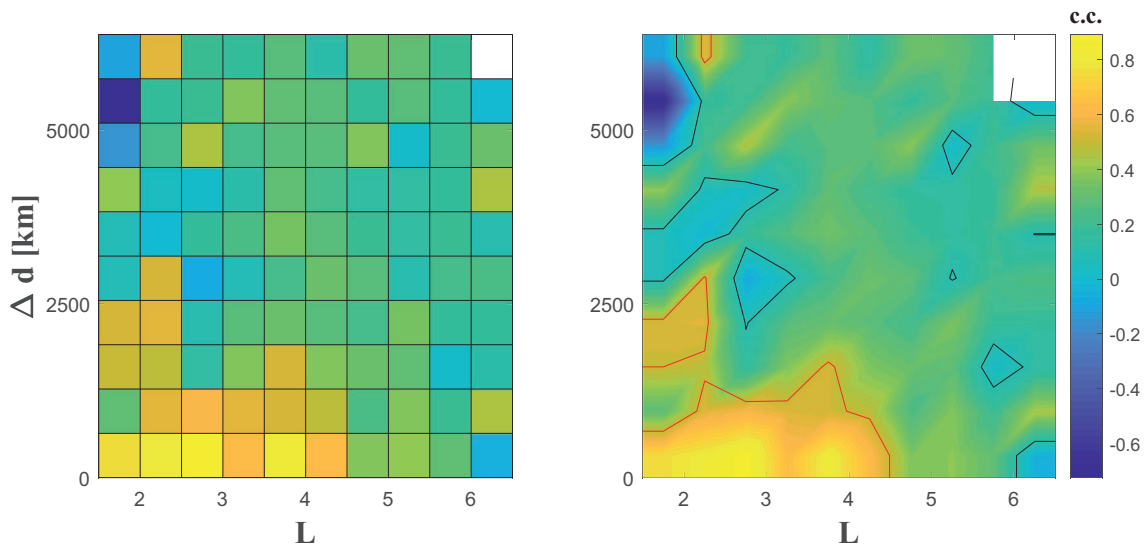


Figure 5. The median spatial correlation coefficients as a function of Δd and L -shell. The red (black) line indicates the 0.5 (0.1) contours.

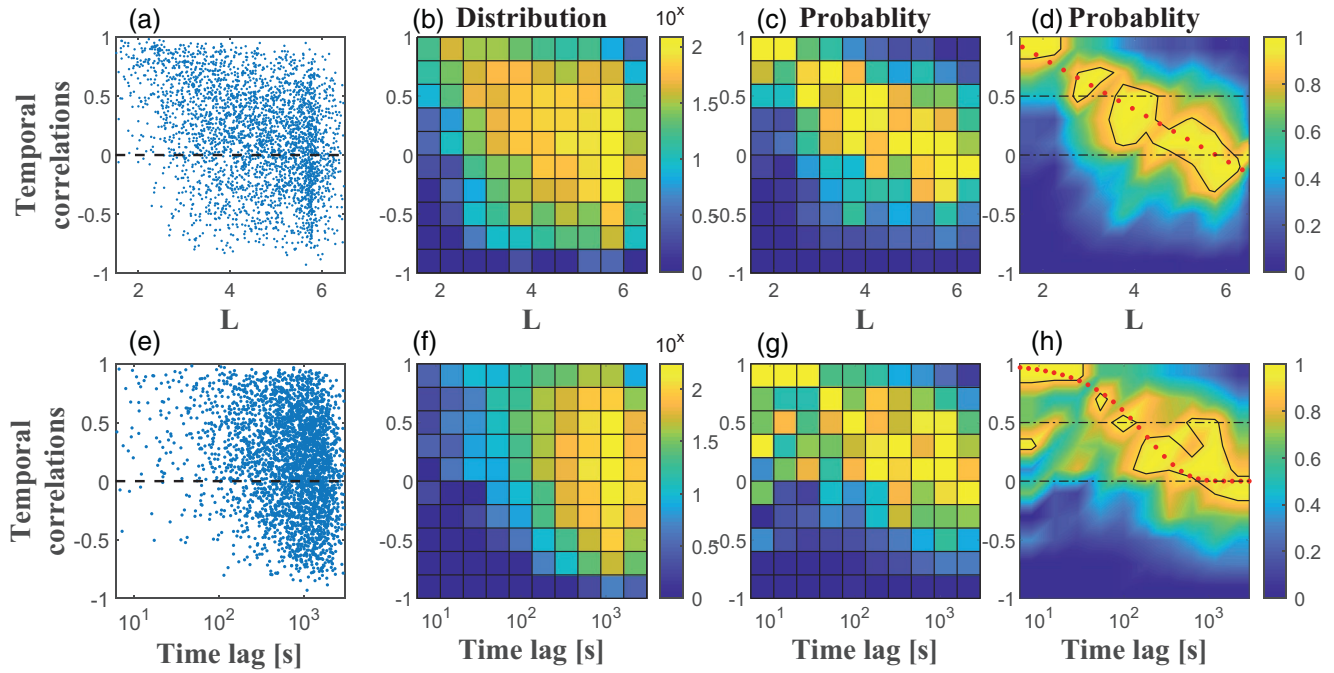


Figure 6. The distributions of the temporal correlation coefficients against L -shell (a–d) and time lag (e–h), which have the same format as Figure 4.

- outside of $L = 3.34$ (Figure 4d)
- when spacecraft are separated by $>1,000$ km (Figure 4h)

And generally incoherent in all other regions (Figure 5)

3.3. Temporal Correlation

The distribution of the temporal correlation coefficients against L -shell and time lag between Van Allen Probes A&B are investigated in Figure 6. Figures 6a–6d show the temporal correlation coefficients in Figure 2h as a function of L -shell, which have the same format as Figures 4a–4d. We find that the temporal correlation coefficients of amplitudes are significantly higher at smaller L -shell than larger L -shell., reaching one when at low $L = 2$, but 0 at $L = 6$, and reaching a correlation coefficient of 0.5 when $L = 3.5$. Figures 6e–6h shows temporal correlation coefficients as a function of the time lag between Van Allen Probes A&B, which have same format and similar variation trend as Figures 4e–4h. It can be seen that as time lag increases, the temporal correlation coefficients of amplitudes decreased significantly. The functional form ($f(\Delta t) = e^{\lambda \Delta t}$) of the fitting is indicated by the red lines in panel h, where $\lambda = -0.0052$ and $R^2 = 0.53$. We find that the temporal correlation coefficients drop to 0.5 when $\Delta t = \sim 2.22$ min. If we consider when the correlation coefficients drop to 0.3 or 0.1 we obtained values of time lag of 3.86 and 7.38 min, respectively. Figures S1e–S1h demonstrate that the ratio of plasmaspheric hiss amplitudes accounting for temporal separation (see Figure 2i) also decreases significantly as the time lag increases.

Figures 7a and 7b show the distributions of the temporal correlation coefficients as a function of the spacecraft time lag and L -shell with the same format as Figure 5. The color indicates the median value of the spatial correlation coefficients in each bin. We can see that when $L < \sim 3$, the temporal correlation coefficient is higher in the smaller L and time lag (drop to 0.5 at averaged $\Delta t \sim 10$ min). When $L > \sim 4.5$, no matter what time lag and L -shell, almost all of the coefficients are reduced to close to 0.

In summary, we find that plasmaspheric hiss is incoherent ($R^2 < 0.5$):

- outside of $L = 3.5$ (Figure 6d)
- when time lag > 2 min (Figure 6h)

And generally incoherent in all other regions (Figure 7)

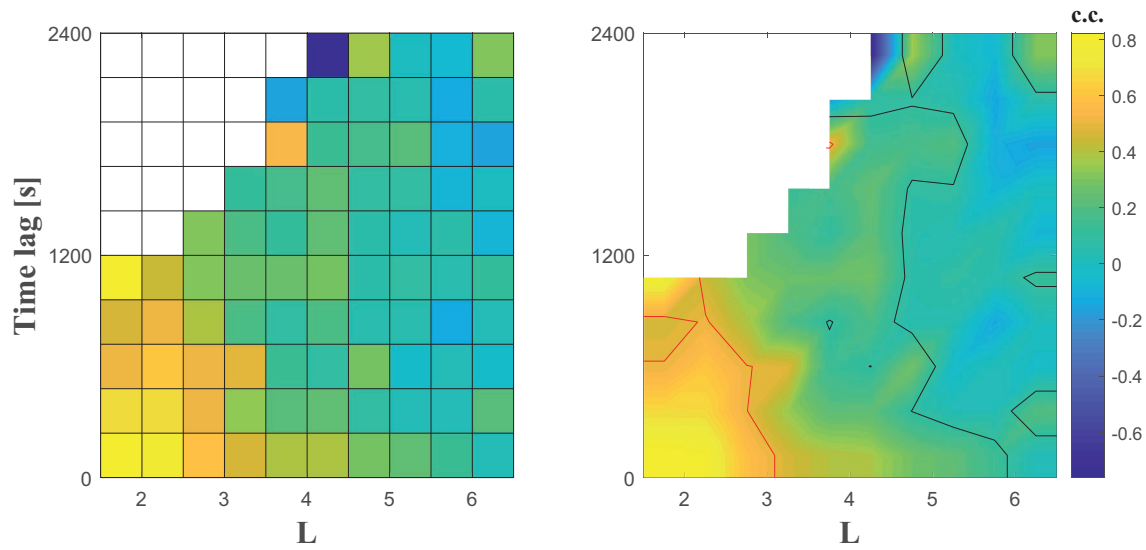


Figure 7. The median temporal correlation coefficients as a function of time lag and L -shell. The red (black) line indicates the 0.5 (0.1) contours.

3.4. Dependence of Correlation on MLT and Substorm Activities

In addition to the L -shell effect, we also investigate the impact of MLT and substorm activities to the global coherence of plasmaspheric hiss, which have been shown to affect the plasmaspheric hiss amplitudes in previous studies (e.g., Meredith et al., 2004). Figure 8 shows that the distributions of spatial and temporal correlation coefficients with respect to (a–c) and (g–i) MLT and (d–f) and (j–l) substorm activity for the spatial and temporal correlations, respectively, in the same format as Figures 4a–4d. The substorm activity is indicated by AL^* , where AL^* is the minimum AL in the previous 3h, which has been shown to be more directly related to substorm activity compared to AE (e.g., McPherron et al., 2013). From Figures 8a–8f, we can see that the spatial-coherent of chorus wave are slightly higher at low AL^* , and there is no clear relationship between the spatial-coherent and MLT; However, no clear relationship was found between the temporal-coherent and AL^* and MLT, as shown in Figures 8g–8l.

4. Discussion

The global coherence of plasmaspheric hiss wave is analyzed statistically using data from the EMFISIS instrument onboard the Van Allen Probes A&B during the period from November 2012 to July 2019. We use established criteria in the literature (e.g., to determine whether measurements are in the plasmaspheric region, the emissions have a broadband structure, and higher planarity and ellipticity) to determine the occurrence and characteristics of plasmaspheric hiss (e.g., Kim et al., 2019; Li et al., 2015, 2010). In total, 3,264 plasmaspheric hiss events with small spacecraft separation ($\Delta d < 1R_E$) are found. In this study, we determine both the spatial and temporal coherence of plasmaspheric hiss events seen by the Van Allen Probe spacecraft. The spatial separation (Δd) between Van Allen Probes A and B is derived along satellite trajectories from equation $\Delta d = \sqrt{\Delta x^2 + \Delta y^2 + \Delta z^2}$ to understand the spatial coherence of hiss inside of the plasmasphere. The temporal separation is estimated as the time lag when Van Allen Probes A and B arriving at the same position to determine the temporal coherence of hiss inside the plasmasphere.

4.1. Spatial Correlation

Figures 4a–4d show that the spatial correlation coefficient is proportional to $-0.115 L + 0.885$, which indicates that hiss waves are less coherent at large L shells. The correlation coefficient reduces to 0.5 (0.3, 0.1)

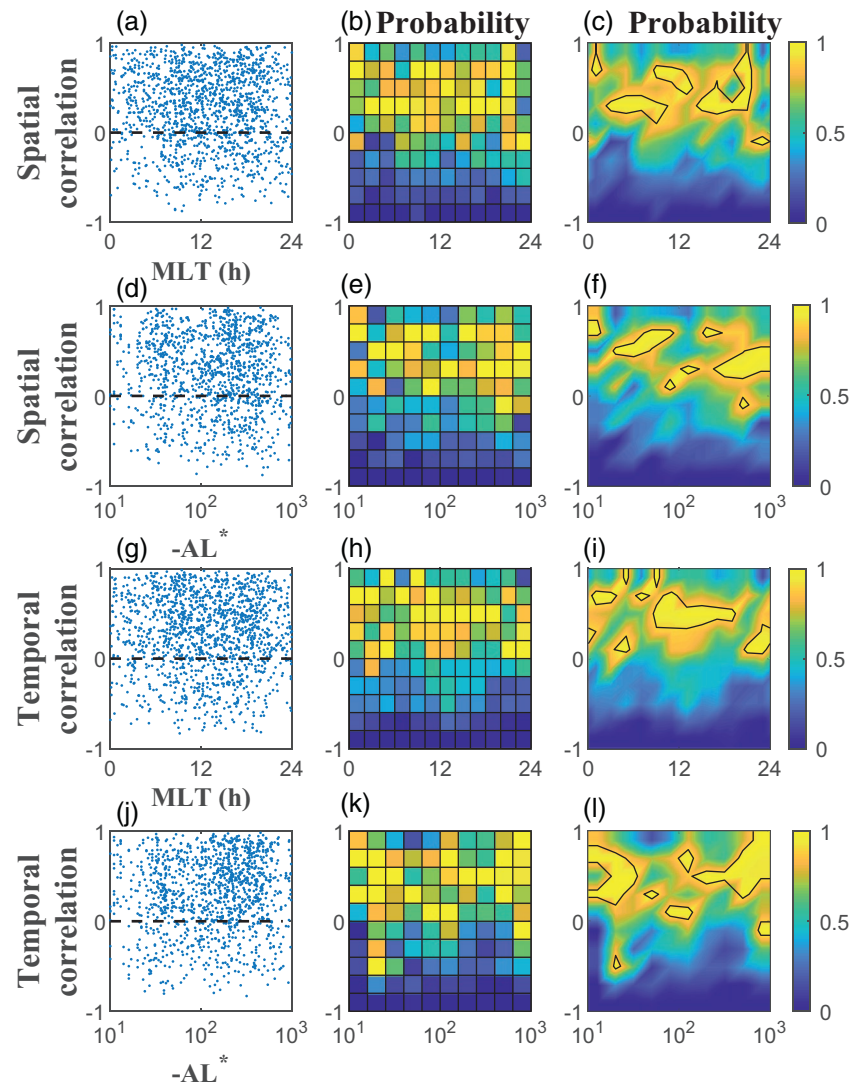


Figure 8. The distributions of the spatial and temporal correlation coefficients against MLT and AL*, which have the similar format to Figures 4a–4d. MLT, magnetic local time.

at ~ 3.34 (5.08, 6.91) and the distributions are very wide, demonstrating a lot of variability in the amount of correlation. Figures 4e–4h show spatial correlation coefficient as a function of Δd ($e^{-6.68 \times 10^{-4} \Delta d}$). The correlation coefficient reduces to 0.5 (0.3, 0.1) when $\sim 1,038$ (1,803, 3,448) km. This suggests that during the construction of drift-averaged diffusion coefficients, it may be important to consider the spatial extent of plasmaspheric hiss more carefully, as measurements of hiss that are less than 0.5 RE apart are not spatially coherent. However, we can see that the event with smallest separation ($\Delta d < \sim 200$ km) is rarely observed, but has a very high coefficient (close to 1).

As in Agapitov et al. (2018), where THEMIS observations were used to study the spatial variability of hiss waves, we find that as spacecraft separation increases, the correlation of hiss waves decreases. However, in Agapitov et al. (2018), the radial correlation of hiss waves decays to 0.5 (0.3) at radial separation $\Delta r \sim 3,000$ (7,000) km, which is significantly larger than our results. In our study, we considered the L variation in coherence when computing the correlation coefficients due to separation in Δd as there is also a natural decay in correlation with L (see Figures 3c and 3d). It is also important to note that the relative spacecraft positions of THEMIS satellites cover a very different range from the Van Allen Probes mission, since Van Allen Probe A catches up and passes Van Allen Probe B every few weeks. This gives us the opportunity to obtain sufficient events with smaller and uniform spatial separation Δd (~ 0.01 – $1 R_E$) to study the Δd effect

on spatial correlation, as shown in Figures 3c and 3d. In our study, we combine the Δd and L effect to the spatial correlation coefficients, as shown in Figure 5, which shows that there is a cutoff in coefficient at a $L = 4.5$ and after that there is no correlation no matter what Δd and L -shell. The possible reason could be that the plasmasphere is more variable near the plasmopause due to the significant and irregular variability in the plasmopause location (e.g., Moldwin et al., 2002; Pedatella et al., 2010). The plasmaspheric hiss will be guided by the density perturbations (e.g., Woodroffe & Streltsov, 2013) and is therefore more likely to be concentrated in regions where the density gradients are favorable.

4.2. Temporal Correlation

As shown in Figures 6a–6d, in general the temporal correlation coefficient decreases with L shell ($-0.217L + 1.254$ for $L > 1.5$). The correlation coefficient reduces to 0.5 (0.3, 0.1) at $L = \sim 3.62$ (4.55, 5.47), which means that the further out in L , the less coherent hiss is in time. We can see that the coefficients at low- L ($L \sim 2$) are very high and hiss is very uniform. Figures 6e–6h show the correlation coefficient is proportional to time lag ($e^{-0.0052^* \Delta t}$). The correlation coefficient reduces to 0.5 (0.3, 0.1) when $\Delta t = \sim 2.2$ (3.86, 7.38) minutes. It should be noted that 10 min is very short in terms of electron diffusion timescales; many radiation belt models assume that hiss amplitudes exist for many hours in the same functional form since the diffusion coefficient models are functions of Kp with 3-h cadence (e.g., Glauert et al., 2013; Shprits et al., 2009)

Temporal correlation coefficients depend on both time lag and L -shell for $L < \sim 3$ (Figure 7). On the other hand, the spatial correlation coefficient drops to 0.5 at about the same $\Delta d \sim 1,500$ km for all $L < 4.5$, as shown in Figure 5. Moreover, no matter what time lag and L -shell, almost all of the correlation coefficients are reduced to nearly 0 at $L > \sim 4.5$ (near the plasmopause), demonstrating that hiss waves observed outside of this region are remarkably localized in MLT and should be considered as such in radiation belt models.

4.3. Generation and Propagation of Hiss

Only $\sim 8\%$ ($\sim 7\%$) spatial (temporal) correlation coefficients with $\Delta d < 1R_E$ are larger than 0.8, which are much lower than expected. This means the plasmaspheric hiss waves are not uniform in plasmasphere. We can only assume that there must be patches of hiss in space and in time, the largest of which exist at low- L . These patches typically exist for less than ~ 10 min and within a region smaller than 1,500 km. Previous studies have brought to light that lower band chorus waves behaves in this way (e.g., Aryan et al., 2016; Nishimura et al., 2011; Shen et al., 2019), but plasmaspheric hiss is often thought to be relatively uniform inside of the plasmasphere (e.g., Delpont et al., 2012; R. M. Thorne et al., 1979). We conclude that the plasmaspheric hiss environment should not be considered a static environment, and statistical averages should be constructed with care. This is especially true since plasmaspheric hiss wave amplitudes exhibit a statistically heavy tail (e.g., Watt et al., 2019, 2021).

Several studies have shown that the plasmaspheric hiss amplitude has a pronounced MLT and substorm activity dependence (e.g., Li et al., 2015; Meredith et al., 2004; Spasojevic et al., 2015), however, we find that there is no significant dependence for spatial or temporal coherence on MLT or substorm activity, as shown in Figure 8. Therefore, MLT and substorm activity only affect the plasmaspheric hiss amplitude, and not the global coherence of the waves, as studied within this study.

Recent numerical experiments have revealed that the temporal variability of wave-particle interactions is important for the solution of Fokker-Planck diffusion models. Watt et al. (2021) shows that results of an idealized numerical diffusion experiment depend sensitively on the timescale of variability of the plasmaspheric hiss diffusion coefficient, which in turn depends on both wave amplitude and local plasma parameters such as number density. For short timescales of variability in the diffusion coefficients (2 min), the solutions of an ensemble of numerical experiments with different randomized selections of diffusion coefficients were very similar to each other, and very similar to the solution obtained if the experiment was run with a single, averaged diffusion coefficient. For long timescales of variability (6 h), the ensemble numerical experiment exhibited a wide range of solutions, none of which were similar to any average of the diffusion coefficients, whether constructed from averaged inputs, or an average of many separately calculated diffusion coefficients. Earlier numerical experiments by Thompson et al. (2020) demonstrated that the solutions of the Fokker-Planck equation for radial diffusion depended sensitively on the timescale of the dif-

fusion—more rapidly varying diffusion coefficients resulted in more diffusion. In both these very different numerical experiments, the variability timescale of the diffusion coefficient describing the wave-particle interactions was an important factor that determined the solution of the Fokker-Planck equation, suggesting that the timescales of variation have universal importance for radiation belt diffusion due to wave-particle interactions.

5. Summary and Conclusions

In conclusion, the plasmaspheric hiss waves are not always spatially or temporally coherent in the plasmasphere. Outside of $L = 4.5$, hiss is statistically both spatially and temporally incoherent, even when the spacecraft is within the plasmasphere. Inside of $L = 4.5$, the plasmaspheric hiss only becomes spatially coherent at remarkably small distances and timescales; when $\Delta d > \sim 1,500$ km or when $\Delta t > \sim 10$ min, plasmaspheric hiss can be considered to be incoherent.

These results have implications for modeling of wave-particle interactions due to plasmaspheric hiss. The construction of averaged models of drift-averaged diffusion coefficients requires knowledge of how the waves vary in space and time. For 1–2 MeV electrons drifting around the Earth at $L < 4.5$, our analysis demonstrates that the temporal coherence lengths are less than the drift period. Knowledge of the distribution of wave amplitudes and plasma parameters (Watt et al., 2019), as well as how they vary, is therefore important to construct an appropriate drift-averaged value of hiss.

This study demonstrates the variation of plasmaspheric hiss amplitudes. In future, additional analysis will demonstrate the temporal and spatial variability of other wave characteristics, such as wave normal angle, as well as plasma number density and magnetic field strength, which are also important input variables to quasilinear diffusion coefficient calculations (Watt et al., 2019). Ultimately, knowledge of the concurrent variability of all inputs into diffusion coefficient calculations is essential to construct a new model of wave-particle interactions that performs averaging in the most appropriate way.

Data Availability Statement

The data that supporting the findings of this study are openly availability at <https://spdf.sci.gsfc.nasa.gov/>.

Acknowledgments

The authors acknowledge the Van Allen Probes project team for EMFISIS data at <https://spdf.sci.gsfc.nasa.gov/>. This work was supported by the National Natural Science Foundation of China (Grants 41731068, 41974189, and 41961130382), the Shandong University (Weihai) Future Plan for Young Scholars (2017WHWLJH08), and the Royal Society Newton Advanced Fellowship (NAF/R1/191047). S. Zhang is supported by the State Scholarship Fund of Chinese Scholarship Council. I. J. Rae is supported by the Science and Technology Facilities Council (Grant ST/V006320/1), and the Natural Environment Research Council (Grants NE/P017150/1, NE/P017185/1, NE/V002554/1, and NE/V002724/1). C. E. J. Watt is supported by STFC grant ST/R000921/1 and NERC grant NE/P017274. X. C. Shen is supported by the NASA grants NNX17AD15 G, 80NSS-C20K0557, 80NSSC20K0698, 80NSS-C20K1270. A. W. Smith is supported by the Science and Technology Facilities Council (Grants ST/S000240/1), and the Natural Environment Research Council (Grants NE/P017150/1 and NE/V002724/1).

References

- Agapitov, O., Krasnoselskikh, V., Zaliznyak, Y., Angelopoulos, V., LeContel, O., & Rolland, G. (2010). Chorus source region localization in the Earth's outer magnetosphere using THEMIS measurements. *Annales Geophysicae*, 28, 1377–1386. <https://doi.org/10.5194/angeo-28-1377-2010>
- Agapitov, O., Mourenas, D., Artemyev, A., Mozer, F. S., Bonnell, J. W., Angelopoulos, V., et al. (2018). Spatial extent and temporal correlation of chorus and hiss: Statistical results from multipoint THEMIS observations. *Journal of Geophysical Research: Space Physics*, 123, 8317–8330. <https://doi.org/10.1029/2018JA025725>
- Aryan, H., Sibeck, D., Balikhin, M., Agapitov, O., & Kletzing, C. (2016). Observation of chorus waves by the Van Allen Probes: Dependence on solar wind parameters and scale size. *Journal of Geophysical Research: Space Physics*, 121, 7608–7621. <https://doi.org/10.1002/2016JA022775>
- Blum, L. W., Agapitov, O., Bonnell, J. W., Kletzing, C., & Wygant, J. (2016). EMIC wave spatial and coherence scales as determined from multipoint Van Allen Probe measurements. *Geophysical Research Letters*, 43, 4799–4807. <https://doi.org/10.1002/2016GL068799>
- Burtis, W. J., & Helliwell, R. A. (1969). Banded chorus—A new type of VLF radiation observed in the magnetosphere by OGO 1 and OGO 3. *Journal of Geophysical Research*, 74(11), 3002–3010. <https://doi.org/10.1029/JA074i011p03002>
- Chan, K.-W., & Holzer, R. E. (1976). ELF hiss associated with plasma density enhancements in the outer magnetosphere. *Journal of Geophysical Research*, 81(13), 2267–2274. <https://doi.org/10.1029/JA081i013p02267>
- Chen, L., Bortnik, J., Li, W., Thorne, R. M., & Horne, R. B. (2012). Modeling the properties of plasmaspheric hiss: 1. Dependence on chorus wave emission. *Journal of Geophysical Research: Space Physics*, 117(A5). <http://dx.doi.org/10.1029/2011ja017201>
- Delport, B., Collier, A. B., Lichtenberger, J., Rodger, C. J., Parrot, M., Clilverd, M. A., & Friedel, R. H. W. (2012). Simultaneous observation of chorus and hiss near the plasmapause. *Journal of Geophysical Research*, 117, A12218. <https://doi.org/10.1029/2012JA017609>
- Dunckel, N., & Helliwell, R. A. (1969). Whistler-mode emissions on the OGO 1 satellite. *Journal of Geophysical Research*, 74(26), 6371–6385. <https://doi.org/10.1029/JA074i026p06371>
- Fok, M. C., Gloer, A., Zheng, Q., Horne, R., Meredith, N., Albert, J., & Nagai, T. (2011). Recent developments in the radiation belt environment model. *Journal of Atmospheric and Solar-Terrestrial Physics*, 73, 1435–1443. <https://doi.org/10.1016/j.jastp.2010.09.033>
- Glauert, S. A., Horne, R. B., & Meredith, N. P. (2013). Three-dimensional electron radiation belt simulations using the BAS radiation belt model with new diffusion models for chorus, plasmaspheric hiss, and lightning-generated whistlers. *Journal of Geophysical Research: Space Physics*, 119, 268–289. <https://doi.org/10.1002/2013JA019281>
- Gurnett, D. A., Anderson, R. R., Scarf, F. L., Fredricks, R. W., & Smith, E. J. (1979). Initial results from the ISEE 1 and 2 plasma wave investigation. *Space Science Reviews*, 23, 103–122.

- Hayakawa, M., Ohmi, N., Parrot, M., & Lefeuvre, F. (1986). Direction finding of ELF hiss emissions in a detached plasma region of the magnetosphere. *Journal of Geophysical Research*, *91*(A1), 135–141. <https://doi.org/10.1029/JA091iA01p00135>
- Kim, K.-C., & Shprits, Y. (2019). Statistical analysis of hiss waves in plasmaspheric plumes using Van Allen Probe observations. *Journal of Geophysical Research: Space Physics*, *124*, 1904–1915. <https://doi.org/10.1029/2018JA026458>
- Kletzing, C. A., Kurth, W. S., Acuna, M., MacDowall, R. J., Torbert, R. B., Averkamp, T., et al. (2013). The electric and magnetic field instrument suite and integrated science (EMFISIS) on Van Allen probes. *Space Science Reviews*, *179*, 127–181. <https://doi.org/10.1007/s11214-013-9993-6>
- Kurth, W. S., Pascuale, S. De, Faden, J. B., Kletzing, C. A., Hospodarsky, G. B., Thaller, S., & Wygant, J. R. (2015). Electron densities inferred from plasma wave spectra obtained by the Waves instrument on Van Allen probes. *Journal of Geophysical Research: Space Physics*, *120*, 904–914. <https://doi.org/10.1002/2014JA020857>
- Li, J., Bortnik, J., Li, W., Thorne, R. M., Ma, Q., Chu, X., et al. (2017). Coherently modulated whistler mode waves simultaneously observed over unexpectedly large spatial scales. *Journal of Geophysical Research: Space Physics*, *122*, 1871–1882. <https://doi.org/10.1002/2016JA023706>
- Li, J., Ma, Q., Bortnik, J., Li, W., An, X., Reeves, G. D., et al. (2019). Parallel acceleration of suprathermal electrons caused by whistler-mode hiss waves. *Geophysical Research Letters*, *46*, 12675–12684. <https://doi.org/10.1029/2019GL085562>
- Li, W., Ma, Q., Thorne, R. M., Bortnik, J., Kletzing, C. A., Kurth, W. S., et al. (2015). Statistical properties of plasmaspheric hiss derived from Van Allen probes data and their effects on radiation belt electron dynamics. *Journal of Geophysical Research: Space Physics*, *120*, 3393–3405. <https://doi.org/10.1002/2015JA021048>
- Li, W., Thorne, R. M., Bortnik, J., Nishimura, Y., Angelopoulos, V., Chen, L., et al. (2010). Global distributions of suprathermal electrons observed on THEMIS and potential mechanisms for access into the plasmasphere. *Journal of Geophysical Research*, *115*, A00J10. <https://doi.org/10.1029/2010JA015687>
- Lyons, L. R., & Thorne, R. M. (1973). Equilibrium structure of radiation belt electrons. *Journal of Geophysical Research*, *78*(13), 2142–2149. <https://doi.org/10.1029/JA078i013p02142>
- Malaspina, D. M., Zhu, H., & Drozdov, A. Y. (2020). A wave model and diffusion coefficients for plasmaspheric hiss parameterized by plasmopause location. *Journal of Geophysical Research: Space Physics*, *125*, e2019JA027415. <https://doi.org/10.1029/2019JA027415>
- Ma, Q., Li, W., Thorne, R. M., Bortnik, J., Kletzing, C. A., Kurth, W. S., & Hospodarsky, G. B. (2016). Electron scattering by magnetosonic waves in the inner magnetosphere. *Journal of Geophysical Research: Space Physics*, *121*, 274–285. <https://doi.org/10.1002/2015JA021992>
- Mauk, B. H., Fox, N. J., Kanekal, S. G., Kessel, R. L., Sibeck, D. G., & Ukhorskiy, A. (2012). Science objectives and rationale for the radiation belt storm probes mission. *Space Science Reviews*, *179*, 3–27. <https://doi.org/10.1007/s11214-012-9908-y>
- McPherron, R. L., Baker, D. N., Pulkkinen, T. I., Hsu, T.-S., Kissinger, J., & Chu, X. (2013). Changes in solar wind-magnetosphere coupling with solar cycle, season, and time relative to stream interfaces. *Journal of Atmospheric and Solar-Terrestrial Physics*, *99*, 1–13. <https://doi.org/10.1016/j.jastp.2012.09.003>
- Meredith, N. P., Horne, R. B., Glauert, S. A., Baker, D. N., Kanekal, S. G., & Albert, J. M. (2009). Relativistic electron loss timescales in the slot region. *Journal of Geophysical Research*, *114*, A03222. <https://doi.org/10.1029/2008JA013889>
- Meredith, N. P., Horne, R. B., Thorne, R. M., Summers, D., & Anderson, R. R. (2004). Substorm dependence of plasmaspheric hiss. *Journal of Geophysical Research*, *109*, A06209. <https://doi.org/10.1029/2004JA010387>
- Moldwin, M. B., Downward, L., Rassoul, H. K., Amin, R., & Anderson, R. R. (2002). A new model of the location of the plasmopause: CRRES results. *Journal of Geophysical Research*, *107*(A11), 1339. <https://doi.org/10.1029/2001JA009211>
- Ni, B., Bortnik, J., Thorne, R. M., Ma, Q., & Chen, L. (2013). Resonant scattering and resultant pitch angle evolution of relativistic electrons by plasmaspheric hiss. *Journal of Geophysical Research: Space Physics*, *118*, 7740–7751. <https://doi.org/10.1002/2013JA019260>
- Ni, B., Li, W., Thorne, R. M., Bortnik, J., Ma, Q., Chen, L., et al. (2014). Resonant scattering of energetic electrons by unusual low-frequency hiss. *Geophysical Research Letters*, *41*, 1854–1861. <https://doi.org/10.1002/2014GL059389>
- Nishimura, Y., Bortnik, J., Li, W., Thorne, R. M., Chen, L., Lyons, L. R., et al. (2011). Multievent study of the correlation between pulsating aurora and whistler mode chorus emissions. *Journal of Geophysical Research*, *116*, A11221. <https://doi.org/10.1029/2011JA016876>
- Némeč, F., Hospodarsky, G., Pickett, J. S., Santolík, O., Kurth, W. S., & Kletzing, C. (2016). Conjugate observations of quasiperiodic emissions by the Cluster, Van Allen Probes, and THEMIS spacecraft. *Journal of Geophysical Research: Space Physics*, *121*, 7647–7663. <https://doi.org/10.1002/2016JA022774>
- Parrot, M., & Lefeuvre, F. (1986). Statistical study of the propagation characteristics of ELF hiss observed on GEOS-1, outside and inside the plasmasphere. *Annales Geophysicae, Series A: Upper Atmosphere and Space Sciences*, *4*, 363–384.
- Pedatella, N. M., & Larson, K. M. (2010). Routine determination of the plasmopause based on COSMIC GPS total electron content observations of the midlatitude trough. *Journal of Geophysical Research*, *115*, A09301. <https://doi.org/10.1029/2010JA015265>
- Santolík, O., & Gurnett, D. A. (2003). Transverse dimensions of chorus in the source region. *Geophysical Research Letters*, *30*(2), 1031. <https://doi.org/10.1029/2002GL016178>
- Santolík, O., Parrot, M., & Lefeuvre, F. (2003). Singular value decomposition methods for wave propagation analysis. *Radio Science*, *38*(1), 1010. <https://doi.org/10.1029/2000RS002523>
- Shen, X.-C., Li, W., Ma, Q., Agapitov, O., & Nishimura, Y. (2019). Statistical analysis of transverse size of lower band chorus waves using simultaneous multisatellite observations. *Geophysical Research Letters*, *46*, 5725–5734. <https://doi.org/10.1029/2019GL083118>
- Shprits, Y. Y., Subbotin, D., & Ni, B. (2009). Evolution of electron fluxes in the outer radiation belt computed with the VERB code. *Journal of Geophysical Research*, *114*, A11209. <https://doi.org/10.1029/2008JA013784>
- Spasojevic, M., Shprits, Y. Y., & Orlova, K. (2015). Global empirical models of plasmaspheric hiss using Van Allen Probes. *Journal of Geophysical Research: Space Physics*, *120*, 10370–10383. <https://doi.org/10.1002/2015JA021803>
- Subbotin, D. A., & Shprits, Y. Y. (2009). Three-dimensional modeling of the radiation belts using the versatile electron radiation belt (VERB) code. *Space Weather*, *7*, S10001. <https://doi.org/10.1029/2008SW000452>
- Summers, D., Ni, B., & Meredith, N. P. (2007). Timescales for radiation belt electron acceleration and loss due to resonant wave-particle interactions: 1. Theory. *Journal of Geophysical Research*, *112*, A04206. <https://doi.org/10.1029/2006JA011801>
- Summers, D., Ni, B., & Meredith, N. P. (2007). Timescales for radiation belt electron acceleration and loss due to resonant wave-particle interactions: 2. Evaluation for VLF chorus, ELF hiss, and electromagnetic ion cyclotron waves. *Journal of Geophysical Research*, *112*, A04207. <https://doi.org/10.1029/2006JA011993>
- Thompson, R. L., Watt, C. E. J., & Williams, P. D. (2020). Accounting for variability in ULF wave radial diffusion models. *Journal of Geophysical Research: Space Physics*, *125*(8), e2019JA027254. <https://doi.org/10.1029/2019JA027254>
- Thorne, R. M., Church, S. R., & Gorney, D. J. (1979). On the origin of plasmaspheric hiss: The importance of wave propagation and the plasmopause. *Journal of Geophysical Research*, *84*(A9), 5241–5247. <https://doi.org/10.1029/JA084iA09p05241>

- Thorne, R. M., Li, W., Ni, B., Ma, Q., Bortnik, J., Baker, D. N., et al. (2013). Evolution and slow decay of an unusual narrow ring of relativistic electrons near $L \sim 3.2$ following the September 2012 magnetic storm. *Geophysical Research Letters*, *40*, 3507–3511. <https://doi.org/10.1002/grl.50627>
- Thorne, R. M., Smith, E. J., Burton, R. K., & Holzer, R. E. (1973). Plasmaspheric hiss. *Journal of Geophysical Research*, *78*(10), 1581–1596. <https://doi.org/10.1029/JA078i010p01581>
- Tsurutani, B. T., & Smith, E. J. (1974). Postmidnight chorus: A substorm phenomenon. *Journal of Geophysical Research*, *79*(1), 118–127. <https://doi.org/10.1029/JA079i001p00118>
- Watt, C. E. J., Allison, H. J., Meredith, N. P., Thompson, R. L., Bentley, S. N., Rae, I. J., et al. (2019). Variability of quasilinear diffusion coefficients for plasmaspheric hiss. *Journal of Geophysical Research: Space Physics*, *124*, 8488–8506. <https://doi.org/10.1029/2018JA026401>
- Watt, C. E. J., Allison, H. J., Thompson, R. L., Bentley, S. N., Meredith, N. P., Glauert, S. A., et al. (2021). The implications of temporal variability in wave-particle interactions in Earth's radiation belts. *Geophysical Research Letters*, *48*, e2020GL089962. <https://doi.org/10.1029/2020GL089962>
- Woodroffe, J. R., & Streltsov, A. V. (2013). Whistler propagation in the plasmopause. *Journal of Geophysical Research: Space Physics*, *118*, 716–723. <https://doi.org/10.1002/jgra.50135>
- Zhima, Z., Cao, J., Liu, W., Fu, H., Yang, J., Zhang, X., & Shen, X. (2013). DEMETER observations of high-latitude chorus waves penetrating the plasmasphere during a geomagnetic storm. *Geophysical Research Letters*, *40*(22), 5827–5832. <https://doi.org/10.1002/2013gl058089>